◇ 基础研究 ◇

http://www.cjcpt.com
2026 Sep; 31(9): 1162-1172

干细胞外泌体介导线粒体与脂肪酸代谢修复肝细胞损伤的作用机制

尹新新[1]，谢昌鹏[1]，李雪静[1]，张丽萍[1]，苏占海[1]，
王海燕[1]，吴　穹[1]，潘元明[2]，安　娟[1]

[1]青海大学医学院基础医学部，西宁 810016，青海；
[2]首都医科大学北京胸科医院肿瘤研究中心，北京 101149

摘要　**目的：**探究脐带间充质干细胞外泌体修复四氯化碳（CCl_4）诱导急性肝损伤的代谢机制，分析关键代谢物在调控修复中的作用。**方法：**实验分为 CCl_4 组、CCl_4+外泌体低剂量组和 CCl_4+外泌体高剂量组，检测各组 HL-7702 的细胞活力，谷草转氨酶（AST）、谷丙转氨酶（ALT）和丙二醛（MDA）的水平，靶向代谢组学分析 CCl_4 组和 CCl_4+外泌体组的差异代谢物，激光共聚焦显微镜观察 HL7702 细胞核和线粒体与外泌体的共定位关系，透射电镜观察各组细胞的线粒体结构变化。**结果：**外泌体在 CCl_4 浓度为 25 mmol/L 时显著逆转了细胞活性下降趋势，外泌体显著降低细胞 AST、ALT 和 MDA 水平，CCl_4 组和 CCl_4+外泌体组共存在 73 种显著差异代谢物，其中包括甘氨脱氧胆酸与十四烷二酸。荧光染色后观察到外泌体与细胞核及线粒体的共定位现象。**结论：**外泌体显著逆转了 CCl_4 诱导的 HL-7702 细胞 AST、ALT 和 MDA 水平异常，并保护线粒体结构和氧化应激损伤。代谢组学结果表明外泌体可能通过介导线粒体与脂肪酸代谢修复肝细胞损伤。

关键词　肝损伤；外泌体；线粒体；脂肪酸代谢；代谢组学

中图分类号：R329.24；R575.1
文献标志码：A
文 章 编 号：1009-2501(2026)09-1162-11
doi: 10.12092/j.issn.1009-2501.2026.09.002

间充质干细胞（mesenchymal stem cells, MSCs）由于其独特的生物学特性，如自我更新、抗氧化、抗纤维化和促进血管新生等，可促进机体多组织脏器的修复，已成为细胞治疗和再生医学的理想种子库[1-3]。其中人脐带间充质干细胞（human umbilical cord mesenchymal stem cells, HUMSCs）具有增殖能力强、免疫原性低、来源方便等优点，这些特性使其易于工业化制备，并有望成为临床应用最具前景的多能干细胞[4]。

研究表明，MSCs 除了通过细胞直接接触和表观调控等方式外，还可以通过旁分泌机制参与肝组织修复[5-6]，如释放多种细胞因子，产生胞外囊泡（主要为外泌体和微泡）及线粒体转移等方式来实现[3]。干细胞外泌体（mesenchymal stem cell-derived exosomes, MSCs-Ex）作为一种天然的纳米载体，转运各种细胞因子和核酸物质，在改善肝脏疾病中具有重要作用，为肝细胞损伤提供了新的治疗思路[7-8]。

急性肝损伤的常见原因包括急性病毒性肝炎、酒精性肝炎、药物性肝炎和感染所致的中毒性肝炎[9]。四氯化碳（CCl_4）是一种毒性有机化合物，属于 2B 类致癌物，可广泛应用于诱导实验动物急性肝损伤、肝纤维化、化学性肝炎、肝癌等模型[10]。因此，本研究采用 CCl_4 建立 HL-7702 肝细胞损伤模型。

本研究旨在评价外泌体对 CCl_4 诱导的急性肝细胞损伤的修复作用，从代谢角度探讨其潜在

2025-10-27 收稿　2026-03-11 修回
国家自然科学基金（82260846）；青海省科技厅应用基础研究项目（2023-ZJ-754）；2023 年度青海省昆仑英才-领军人才项目
尹新新，女，硕士研究生，研究方向：高原医学。
E-mail: xinxin991209@163.com
安娟，通信作者，女，博士，博士生导师，研究方向：高原医学，胃癌。
E-mail: anjuan@qhu.edu.cn
潘元明，共同通信作者，男，博士，博士生导师，研究方向：干细胞。
E-mail: peterfpan2020@mail.ccmu.edu.cn

的调控机制，为临床治疗提供新的策略。

1　材料与方法

1.1　主要试剂和仪器　CCl_4（Standard for GC, ≥ 99.9%, GC, 水封）购于上海麦克林生化科技股份有限公司。CCK-8 试剂，BCA 蛋白浓度测定试剂盒，谷草转氨酶（AST）、谷丙转氨酶（ALT）和丙二醛（MDA）比色法试剂盒购于武汉伊莱瑞特生物科技股份有限公司。DiR 碘化物荧光探针购于北京瑞泰生物有限公司。线粒体绿色荧光探针购于上海碧云天生物技术有限公司。Hoechst-33342 细胞核染料购于上海碧云天生物技术有限公司。CO_2 恒温培养箱（Thermo Fisher Scientific Inc.）。NanoSight LM10-HS 系统（NanoSight Ltd）。酶标仪（VICTOR Nivo, Revivity）。共聚焦显微镜（AXR with NSPARC, Nikon）。

1.2　HUMSCs 培养体系　细胞来源与培养条件：HUMSCs 购自中国医学科学院肿瘤研究所，使用北京优康生物技术有限公司提供的 GMP 级无血清间充质干细胞培养基（产品编号：NC0106/NC0106s）。培养体系置于恒温培养箱中，维持 37℃、5% CO_2 的标准培养环境。伦理审查：本研究经北京胸科医院机构审查委员会批准（批件号：2022-043），实验过程严格遵循《赫尔辛基宣言》制定的伦理准则。

1.3　外泌体的分离、表征与鉴定　细胞培养与样本制备：将 5×10^6 个 HUMSCs 接种于 100 mm 培养皿，使用含 10% 外泌体去除血清（exosome-depleted FBS）、2 mmol/L-谷氨酰胺及抗生素的 DMEM 培养基培养。48 h 后收集条件培养基，1 500 r/min 离心 25 min 去除细胞碎片。超速离心纯化：上清液经 0.22 μm 滤膜过滤后，于 4℃ 环境下 150 000×*g* 超速离心 2 h（Beckman Coulter 离心机），沉淀用 PBS 重悬。外泌体蛋白浓度通过 Pierce BCA 蛋白检测试剂盒定量。纳米颗粒追踪分析：采用 NanoSight LM10-HS 系统检测囊泡粒径分布，仪器经聚苯乙烯微球校准。通过 NTA 2.3 软件分析视频数据，计算外泌体浓度及粒径。标志蛋白检测：Western blot 验证外泌体标志蛋白（CD9、CD63、CD81）及内参蛋白 TSG101，同时检测阴性标志物 Calnexin。结构表征：透射电镜（TEM）负染技术观察外泌体形貌。

1.4　正常人肝细胞系培养体系　人胚胎肝细胞系 HL7702 购自上海冠导生物工程有限公司，培养于含 15% 热灭活胎牛血清（FBS）和 1% 青霉素-链霉素双抗溶液的 RPMI1640 培养基中，置于 37℃、5% CO_2 及饱和湿度的培养箱内培养。细胞传代与实验处理：传代标准：细胞密度达到 0.8×10^6 ~ 1.0×10^6 cells/mL 时进行传代。消化方法：对数生长期细胞使用 0.25% 胰蛋白酶+0.02% EDTA 消化后用于后续实验。

1.5　细胞活性　将 HL7702 细胞接种于 96 孔板（3×10^3 cell/well, 100 μL/well），分为 CCl_4 组、CCl_4+外泌体低剂量组（11.7×10^6 particulate/well）和 CCl_4+外泌体高剂量组（23.4×10^6 particulate/well）。细胞接种时加入外泌体。培养 24 h 后，加入含 CCl_4（100 μL/well）的完全培养基。CCl_4 溶解于无水乙醇（终浓度<0.5%）中，在冰浴条件下用超声波细胞破碎机溶解。继续培养 24 h 后，加入 CCK-8 试剂，2 h 后用酶标仪测定 450 nm 处的吸光度，计算细胞活力，所有实验重复 3 次进行数据分析。

1.6　细胞 AST、ALT 和 MDA 检测　将 HL7702 细胞接种于 100 mm 培养皿（3×10^6 cell/dish），分为：空白对照组，CCl_4 模型组，CCl_4+外泌体干预组（1.4×10^9 particulate/dish）。培养 24 h 后，向 CCl_4 组及 CCl_4+外泌体干预组加入 CCl_4 溶液（终浓度 25 mmol/L，无水乙醇终浓度<0.5%）。继续培养 24 h，冰浴条件下采用超声细胞破碎仪匀浆。BCA 蛋白浓度测定试剂盒检测细胞匀浆总蛋白浓度。比色法试剂盒检测细胞匀浆中的肝损伤标志物：AST 和 ALT。氧化应激指标：酶标仪测定 510 nm（AST/ALT）及 532 nm（MDA）吸光度值。数据以 μmol/mg prot 为单位标准化。

1.7　细胞靶向代谢组学检测　将 HL7702 细胞接种于 100 mm 培养皿（3×10^6 cell/dish，终体积 6 mL），分为：CCl_4 模型组，CCl_4+外泌体干预组（1.4×10^9 particulate/dish）。细胞接种时加入外泌体，CCl_4 终浓度为 25 mmol/L。使用细胞刮板收集细胞并送至武汉迈维代谢生物科技股份有限公司进行液相色谱串联质谱（LC-MS/MS）检测。数据采集仪器系统主要包括超高效液相色谱（ultra performance liquid chromatography, UPLC）（ExionLC™ AD, https://sciex.com.cn/）和串联质谱（tandem mass spectrometry, MS/MS）（QTRAP®

6500+, https://sciex.com.cn/)。采用 Analyst 1.6.3 软件处理质谱数据，采用 MultiQuant 3.0.3 软件处理质谱数据。

1.8 细胞线粒体结构检测 将 HL7702 细胞接种于 100 mm 培养皿(3×10⁶ cell/dish)，分为：CCl_4模型组，CCl_4+外泌体干预组(1.4×10⁹ particulate/dish)。细胞接种时加入外泌体，CCl_4终浓度为 25 mmol/L。收集细胞固定液固定并送检(北京中科百测技术服务有限公司)。

1.9 细胞荧光共定位分析 将 HL7702 细胞接种于 35 mm 共聚焦培养皿中(1.5×10⁵ cell/dish)，分为 DiR-PBS 对照组与 DiR+外泌体实验组。实验组预先将 DiR 碘化物荧光探针与外泌体于 37℃ 孵育 15 min，随后转移至培养皿中继续共培养 24 h。培养结束后，弃去两组上清液，用 PBS 洗涤细胞 3 次，加入线粒体绿色荧光探针 37℃ 避光标记 30 min，再次 PBS 洗涤 3 次后，用 Hoechst-33342 细胞核染料 37℃ 染色 15 min。最终经 PBS 洗涤，使用共聚焦显微镜进行多通道荧光成像观察。

1.10 统计学方法 使用 GraphPad Prism 10 软件进行数据统计。两组间数据和多组间数据分析分别使用独立样本 *t* 检验和单因素方差分析。

2 结果

2.1 HUMSCs 及其外泌体表征鉴定 流式细胞术检测到 HUMSCs 阳性表面标志物 CD29、CD44、CD90 和 CD105，未检测到阴性表面标志物 CD34 和 CD45(Fig.1A)。镜下观察 HUMSCs 呈长梭形、成纤维细胞样(Fig.1B)。成骨诱导和成脂诱导表明 HUMSCs 具有多向分化潜能。纳米颗粒跟踪分析检测外泌体粒径分布，主要范围在 50～200 nm。透射电镜观察到外泌体双层膜、茶托状的囊泡结构。蛋白印迹结果显示外泌体表面标志物 CD9、CD63、CD81 和腔内蛋白 TSG101 呈阳性，阴性标记物 Calnexin 未检出(Fig.1C)。

2.2 外泌体干预 CCl_4 诱导的肝细胞活性检测 利用 CCK-8 实验通过细胞活性实验评估高、低剂量干细胞外泌体的干预效果(Fig.2)。其中，CCl_4 组中，随着 CCl_4 浓度升高，细胞活性显著降低。当 CCl_4 浓度为 25 mmol/L 时，高剂量外泌体组(23.4×10⁶ particulate/well)与低剂量外泌体组(11.7×10⁶ particulate/well)均较 CCl_4 组展现出治疗效应，显著逆转了细胞活性下降趋势，且高剂量组的治疗效果优于低剂量组。但在 CCl_4 浓度达到 30 mmol/L 时，两组均无法逆转活性下降。

2.3 细胞损伤标志物 AST、ALT 及 MDA 分析 检测外泌体对 CCl_4 诱导肝细胞损伤中 AST、ALT 及 MDA 水平的影响(Fig.3)。与空白组相比，CCl_4 组的 AST、ALT 和 MDA 水平均显著升高(P<0.05)；而与 CCl_4 组相比，CCl_4+外泌体组的 AST、ALT 和 MDA 水平均显著降低(P<0.05)。

2.4 细胞靶向代谢组学 本研究使用数据采集仪器系统主要包括超高效液相色谱和串联质谱，靶向组别 T500(包含糖类、氨基酸和能量代谢相关)。基于标准品构建 MWDB(Metware Database)数据库并利用三重四级杆质谱的多反应监测模式(multiple reaction monitoring, MRM)对检测数据进行定性和定量分析。利用多元统计分析方法对高维复杂数据进行简化和降维，同时保留原始信息，建立可靠的数学模型以总结研究对象的代谢谱特征。通过主成分分析(PCA)初步了解样本组间整体代谢差异及组内变异性，并进一步利用正交偏最小二乘判别分析(OPLS-DA)阐明 CCl_4 模型组和 CCl_4+外泌体干预组(1.4×10⁹ particulate/dish)的代谢差异(Fig.4)。

基于 OPLS-DA 模型(生物学重复≥3)得到的变量重要性投影(variable importance in projection, VIP)，初步筛选出组间差异的代谢物。同时结合单变量分析的 *P*-value/FDR(生物学重复≥2)和 FC 值来进一步筛选出差异代谢物。筛选出两组间显著差异代谢物共 73 种，其中 CCl_4 组较 CCl_4+外泌体组上调 55 种、下调 18 种。显著上调代谢物包括甘氨脱氧胆酸、脱氧胆酸、胆酸；显著下调代谢物包括维生素 B3 和 2,3-二磷酸甘油酸(Tab.1)。

基于筛选标准鉴定得到的差异代谢物，选择在 OPLS-DA 模型中 VIP 值最大的前 50 个代谢物进行展示(Fig.5A)。对应用筛选标准鉴定得到的差异代谢物的原始含量按行采用归一化处理(unit variance scaling, UV Scaling)并聚类(Fig.5B)。根据差异代谢物结果，进行 KEGG 通路富集(Fig.5C)，标注的主要代谢通路包括初级胆汁酸生物合成(primary bile acid biosynthesis)。

2.5 荧光共定位分析 采用共聚焦显微镜观

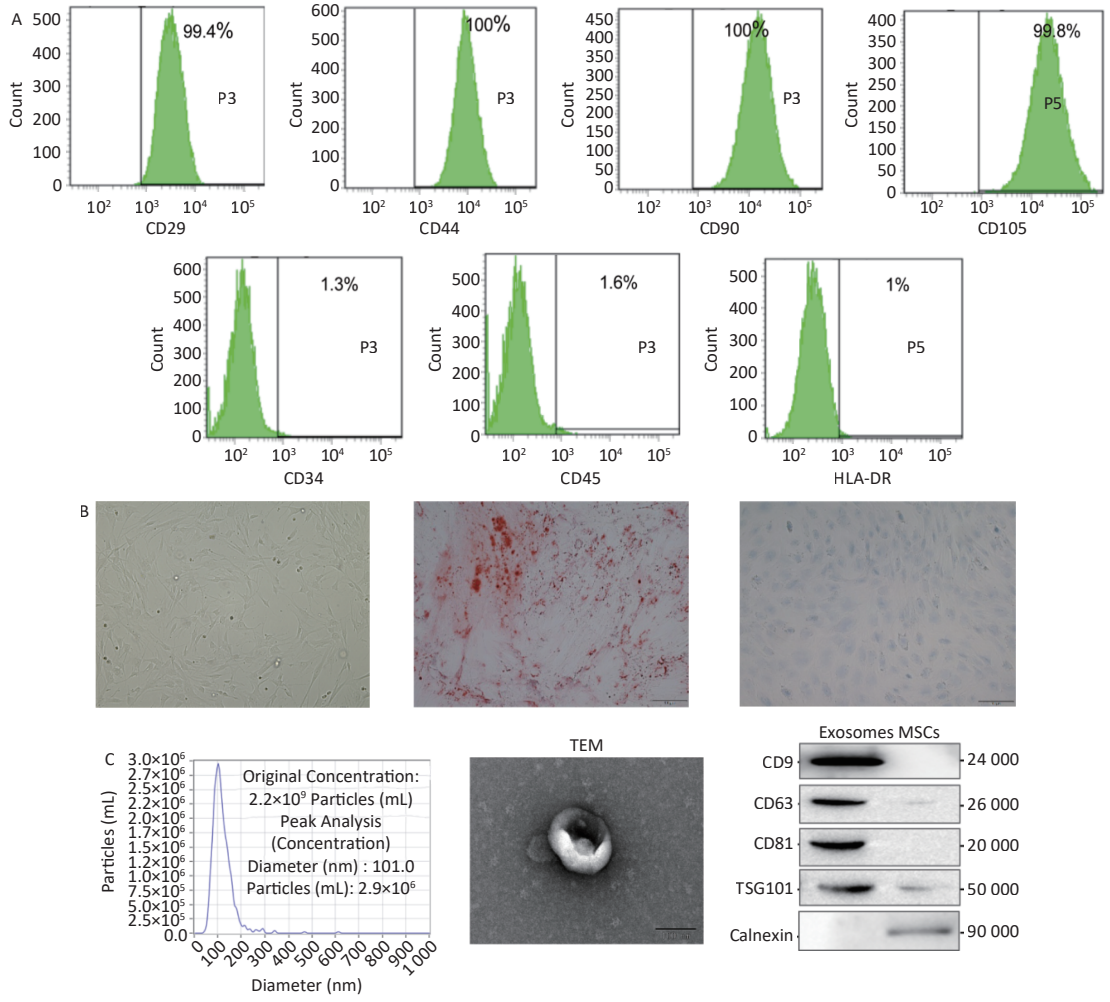


Fig.1　Identification and characterization of human umbilical cord-derived mesenchymal stem cells and their-derived exosomes

A: flow cytometry detection of MSC surface markers: HUMSCs exhibit high expression of CD29, CD44, CD90, and CD105, while low expression of CD34, CD45, and HLA-DR. B: morphology and multipotential differentiation potential of live HUMSCs (left: uninduced HUMSCs exhibit spindle and fibroblast-like morphological characteristics, 10×; middle: oil red O staining indicates adipogenic differentiation; right: Alcian blue staining indicates osteogenic differentiation). All data are from three independent experiments. C: Characterization and identification of stem cell-derived exosomes: nanoparticle tracking analysis (NTA): determination of exosome particle size distribution (50-200 nm) and concentration. Western blotting (WB): detection of exosome surface markers (CD9, CD63, CD81) and intracellular protein TSG101, with negative marker calnexin not detected, confirming exosome purity. Transmission electron microscopy (TEM): negative staining reveals a typical bilayer membrane structure and cup-like morphology.

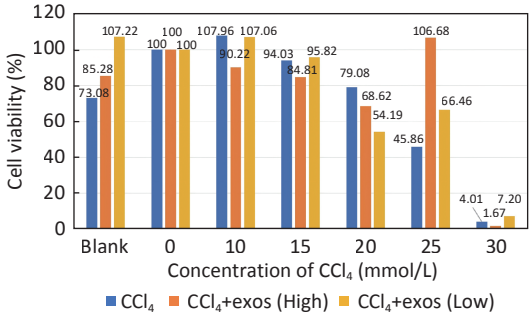


Fig.2　Both low-dose and high-dose exosome treatments exhibited significant therapeutic effects

察到外泌体与细胞核及线粒体的共定位现象（Fig.6A）。其中：蓝色标记细胞核，绿色标记线粒体，红色标记外泌体。在 DiR 组中，DiR 染料进入细胞后未能与线粒体共定位，红色信号与绿色信号清晰可辨，区别分明；而在 DiR+外泌体组中，红色信号与绿色信号明显重叠呈现橙黄色，表明经 DiR 标记的外泌体在线粒体处富集。通过增加 *Z* 轴观察，进一步证实外泌体存在于细胞内部。

2.6　细胞线粒体结构　使用透射电镜观察各组线粒体结构。与空白组相比，CCl_4 组线粒体呈现皱缩状态，且嵴结构消失；而在 CCl_4+外泌体组中观察到线粒体损伤得到显著改善（Fig.6B）。

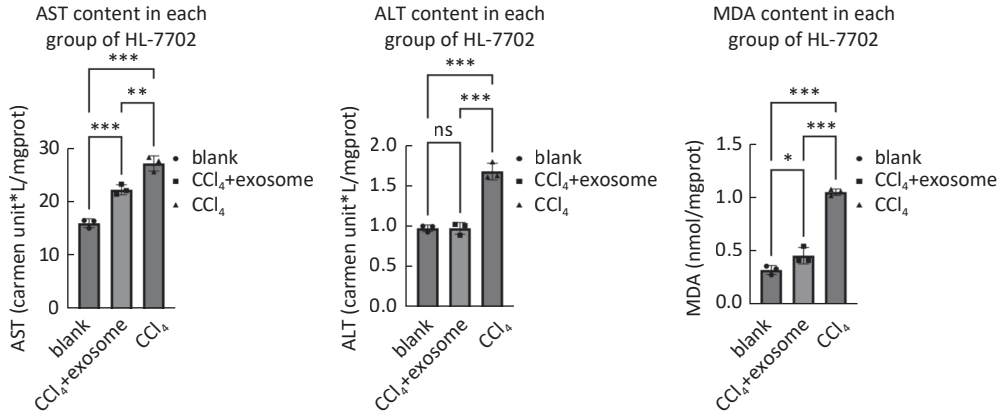


Fig.3 Detection of hepatocyte injury markers in homogenates of HL-7702 cells in each group ($\bar{x} \pm s$, n=3)

ns: P>0.05, *: P<0.05, **: P<0.01, ***: P<0.001.

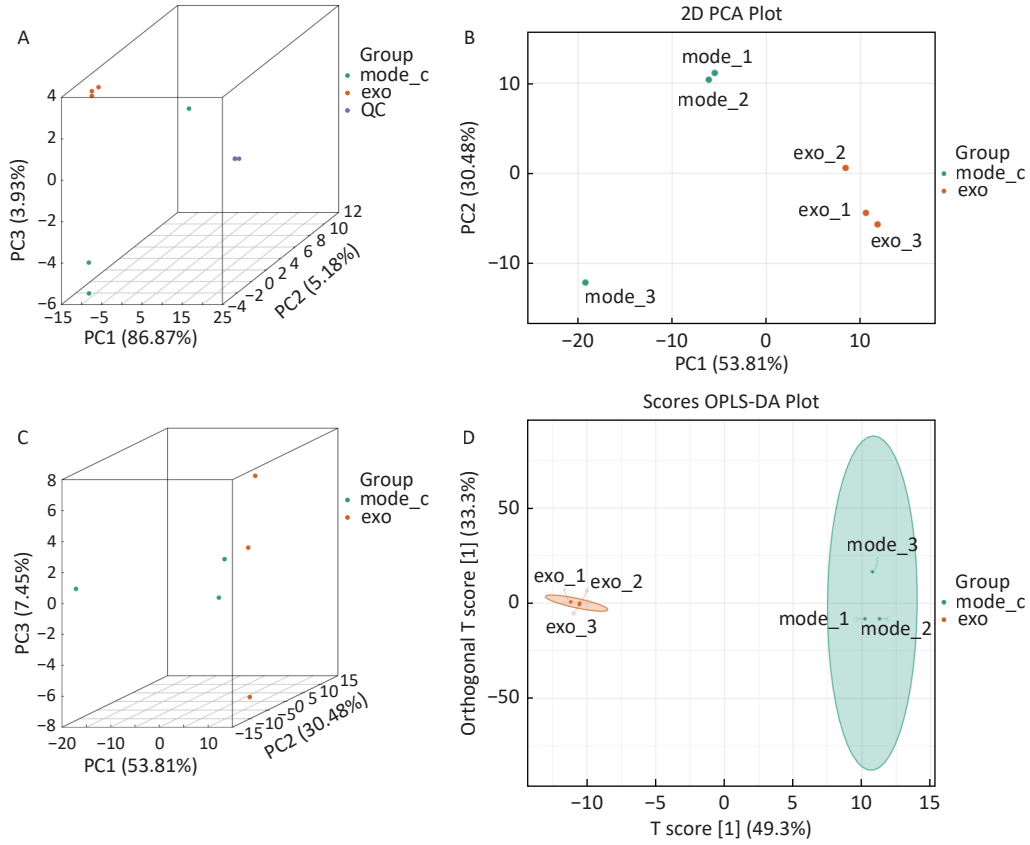


Fig.4 Metabolomic PCA and OPLS-DA analysis

A: 3D-PCA score plot of mass spectrometry data from each group. mode_c: CCl_4 model group; exo: CCl_4+exosome intervention group; QC: quality control group (mixed solution from each group); the same below PC1 represents the first principal component, PC2 represents the second principal component, and the percentage indicates the explanatory power of that principal component to the dataset; each point in the figure represents a sample, and samples from the same group are represented by the same color. B: grouped 2D-PCA analysis plot. C: grouped 3D-PCA analysis plot. D: OPLS-DA score plot. The abscissa represents the predictive principal component, and the direction of the abscissa indicates the differences between groups; the ordinate represents the orthogonal principal component, and the direction of the ordinate indicates the differences within groups; the percentage indicates the explanatory power of that component to the dataset.

3 讨论

肝细胞作为肝脏中数量最多的细胞类型，在糖异生、脂质生成和谷氨酰胺合成等合成代谢，以及糖酵解、脂解和尿素生成等分解代谢活动中均具有高度特异性。线粒体在这些生化过程中均

Tab.1 Differential metabolite table (CCl_4 group *vs.* CCl_4+exosome group)

Compounds	Class	VIP	*P* value	FDR	Fold Change	Log2FC	Type
4-Guanidinobutanoic acid	Organic acids and their derivatives	1.124	0.122	0.284	3.364	1.750	Up
Oleoylethanolamide	Lipid amide	1.341	0.006	0.116	2.321	1.215	Up
Trigonelline	Coenzyme and vitamin	1.352	0.023	0.140	6.466	2.693	Up
Betaine	other	1.177	0.086	0.239	2.366	1.243	Up
Deoxycholic acid	Bile acid	1.416	0.001	0.038	2.540	1.345	Up
Betaine aldehyde chloride	Other	1.387	0.001	0.038	2.208	1.143	Up
Oleylcarnitine	Acylcarnitine	1.401	0.007	0.116	4.905	2.294	Up
DL-carnitine	Acylcarnitine	1.386	0.010	0.116	3.105	1.635	Up
Acetyl-carnitine	Acylcarnitine	1.121	0.124	0.285	2.802	1.486	Up
Myristoyl-L-carnitine	Acylcarnitine	1.321	0.038	0.166	2.837	1.504	Up
L-palmitoylcarnitine	Acylcarnitine	1.415	0.002	0.054	5.234	2.388	Up
Stearoyl-carnitine	Acylcarnitine	1.421	0.000	0.001	6.883	2.783	Up
Taurine	Sulfonic acid compounds	1.037	0.167	0.331	5.679	2.506	Up
N6-threonylcarbamoyladenosine	Nucleotides and their metabolites	1.295	0.041	0.166	2.150	1.104	Up
2'-O-methylcytidine	Nucleotides and their metabolites	1.411	0.000	0.012	2.490	1.316	Up
5'-Deoxy-5'-methylthioadensine	Nucleotides and their metabolites	1.041	0.161	0.325	2.377	1.249	Up
2'-O-methyluridine	Nucleotides and their metabolites	1.352	0.017	0.125	2.701	1.434	Up
5,2'-O-dimethyluridine	Nucleotides and their metabolites	1.320	0.037	0.166	5.325	2.413	Up
Pseudouridine	Nucleotides and their metabolites	1.319	0.041	0.166	2.305	1.205	Up
Uric acid	Purine and pyrimidine	1.004	0.187	0.336	6.589	2.720	Up
N,N-Dimethylguanosine	Nucleotides and their metabolites	1.255	0.066	0.204	2.725	1.446	Up
Thyroxine	Hormones and hormone-related substances	1.352	0.019	0.128	2.129	1.090	Up
Prostaglandin E2(PGE2)	Hormones and hormone-related substances	1.043	0.145	0.303	2.142	1.099	Up
Acetoacetic acid sodium salt	Organic acids and their derivatives	1.351	0.013	0.122	2.248	1.169	Up
Fumaric acid	Organic acids and their derivatives	1.242	0.069	0.206	2.694	1.430	Up
3-methylcytidine	Nucleotides and their metabolites	1.206	0.036	0.166	2.719	1.443	Up
Cyclic-AMP	Nucleotides and their metabolites	1.104	0.140	0.300	2.696	1.431	Up
Pyridoxine	Pyridine and its derivatives	1.088	0.140	0.300	19.293	4.270	Up
N-Palmitoylglycine	Amino acid derivatives	1.223	0.074	0.216	2.003	1.002	Up
N-A-Acetyl-L-Arginine	Amino acid derivatives	1.279	0.016	0.125	2.783	1.477	Up
4-Aminobutyric Acid	Amino acid derivatives	1.349	0.025	0.147	4.746	2.247	Up
Beta-Alanine	Amino acid derivatives	1.144	0.114	0.280	5.453	2.447	Up

Continued from Tab. 1

Compounds	Class	VIP	*P* value	FDR	Fold Change	Log2FC	Type
L-Cystine	Amino acid	1.210	0.065	0.201	2.033	1.024	Up
Ribonic acid	Sugar acid	1.376	0.016	0.125	3.987	1.995	Up
Sphinganine	Amines	1.067	0.150	0.306	2.719	1.443	Up
gama-Glutamate-Cysteine	Small peptide	1.130	0.121	0.284	2.084	1.059	Up
Trans-4-Hydroxy-L-Proline	Amino acid derivatives	1.086	0.140	0.300	7.293	2.867	Up
Stachydrine hydrochloride	Organic acids and their derivatives	1.229	0.063	0.200	11.336	3.503	Up
Anserine	Small peptide	1.100	0.108	0.270	3.582	1.841	Up
Indolelactic acid	Indole and its derivatives	1.076	0.117	0.283	7.036	2.815	Up
1-Methyladenine	Nucleotides and their metabolites	1.385	0.016	0.125	Inf	Inf	Up
Myo-Inositol	Alcohol and polyol	1.023	0.172	0.336	Inf	Inf	Up
5-hydroxymethylcytidine	Nucleotides and their metabolites	1.277	0.052	0.186	Inf	Inf	Up
Glycodeoxycholic acid	Bile acid	1.422	0.001	0.038	Inf	Inf	Up
Allantoin	Imidazoles	1.258	0.064	0.201	Inf	Inf	Up
Arachidonylcarnitine	acylcarnitine	1.401	0.009	0.116	Inf	Inf	Up
Glycolithocholic acid	Bile acid	1.416	0.002	0.060	Inf	Inf	Up
Dodecanoylcarnitine	Acylcarnitine	1.161	0.106	0.270	Inf	Inf	Up
Deoxyuridine	Nucleotides and their metabolites	1.006	0.184	0.336	Inf	Inf	Up
Salicylic acid	Benzene and its derivatives	1.006	0.185	0.336	Inf	Inf	Up
3-hydroxymethylglutaric acid	Amino acid derivatives	1.002	0.188	0.336	Inf	Inf	Up
7a,27-Dihydroxycholesterol	Hormones and hormone-related substances	1.003	0.188	0.336	Inf	Inf	Up
Cholic acid	bile acid	1.005	0.184	0.336	Inf	Inf	Up
L-Cystathionine	Amino acid derivative	1.006	0.184	0.336	Inf	Inf	Up
3-Hydroxy-9-hexadecenoyl-L-carnitine	Acylcarnitine	1.006	0.184	0.336	Inf	Inf	Up
Vitamin B3	Coenzyme and vitamin	1.072	0.142	0.301	0.479	−1.061	Down
Tridecanedioic acid	Fatty acyl	1.286	0.050	0.182	0.413	−1.275	Down
Tetradecanedioic acid	Fatty acyl	1.331	0.030	0.159	0.394	−1.343	Down
Thiamine pyrophosphate	Coenzyme and vitamin	1.378	0.001	0.038	0.361	−1.471	Down
BPG	Phosphoric acid compounds	1.185	0.037	0.166	0.421	−1.248	Down
2-Picolinic Acid	Pyridine and its derivatives	1.166	0.096	0.250	0.426	−1.233	Down
Gly-Trp	Small peptide	1.255	0.055	0.188	0.392	−1.350	Down
Phe Leu	Small peptide	1.315	0.009	0.116	0.413	−1.275	Down
N,N-dimethylarginine	Amino acid derivatives	1.401	0.007	0.116	0.142	−2.819	Down

Continued from Tab. 1

Compounds	Class	VIP	*P* value	FDR	Fold Change	Log2FC	Type
L-Alanyl-L-proline	Small peptide	1.288	0.032	0.159	0.474	−1.077	Down
Gly-Val	Small peptide	1.286	0.014	0.125	0.316	−1.661	Down
Mannitol	Sugar alcohol	1.208	0.060	0.196	0.424	−1.239	Down
Ser-Glu	Small peptide	1.342	0.019	0.128	0.311	−1.683	Down
Thr-Leu	Small peptide	1.294	0.012	0.121	0.452	−1.146	Down
Phe Val	Small peptide	1.319	0.014	0.125	0.351	−1.509	Down
Dodecanedioic Acid	Fatty acyl	1.226	0.027	0.152	0.304	−1.716	Down
Adenine	Nucleotides and their metabolites	1.139	0.087	0.239	0.120	−3.062	Down
Benzoic acid	Benzene and its derivatives	1.016	0.184	0.336	0.000	−Inf	Down

Select metabolites with a VIP (variable importance in projection) value greater than 1. The VIP value indicates the impact strength of the inter-group difference of the corresponding metabolite in the classification and discrimination of each group of samples. Metabolites with a VIP value greater than 1 are generally considered to have significant differences. Select metabolites with a fold change greater than or equal to 2 and a fold change less than or equal to 0.5. Metabolites with a difference of more than 2 times or less than 0.5 times between the two groups are considered to have significant differences.

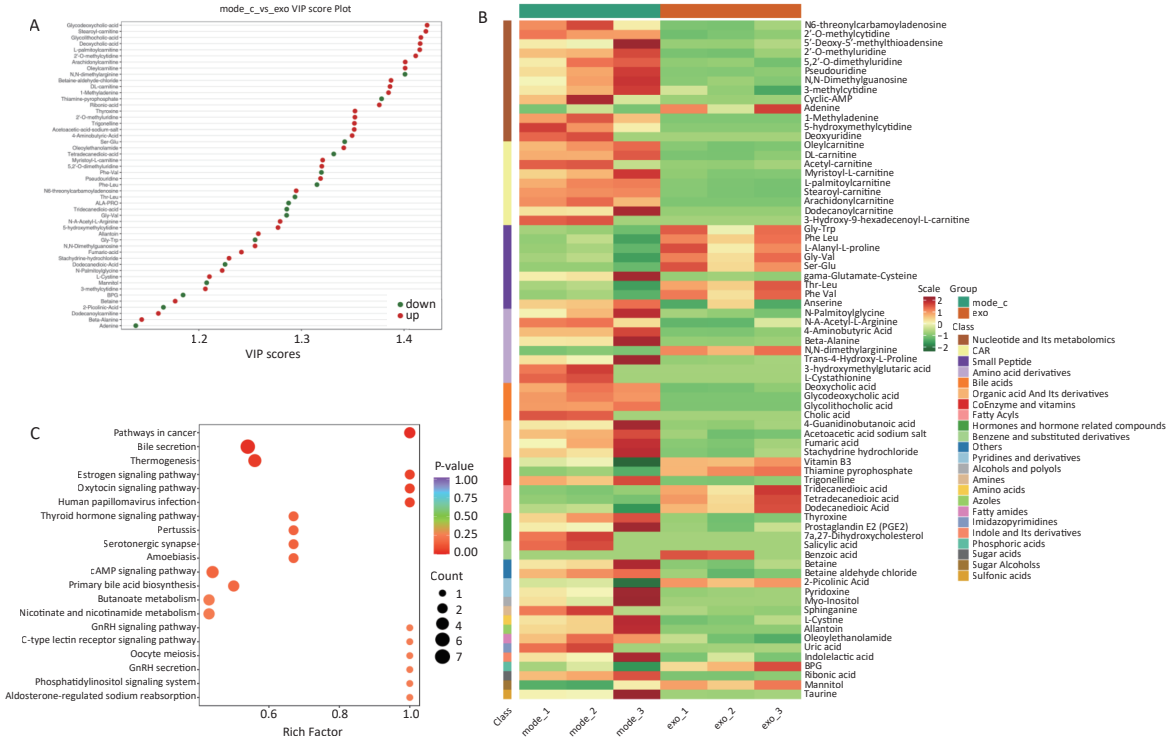


Fig.5 Clustering and KEGG enrichment of differential metabolites in the CCl_4 group and CCl_4+exosome group

A: VIP value plot of differential metabolites. The x-axis represents the VIP value, and the y-axis represents metabolites. Red represents upregulated differential metabolites, and green represents downregulated differential metabolites. B: Heatmap of differential metabolite clustering. The horizontal axis represents sample names, and the vertical axis represents metabolite information. Scale represents the expression level after normalization (the redder the color, the higher the expression level; the greener the color, the lower the expression level). Group represents the grouping, and Class represents the substance classification. C: KEGG enrichment plot of differential metabolites. The x-axis represents the Rich factor corresponding to each pathway, and the y-axis represents the pathway name. The color of the points represents the *P*-value, with red indicating more significant enrichment. The size of the points represents the number of differential metabolites enriched.

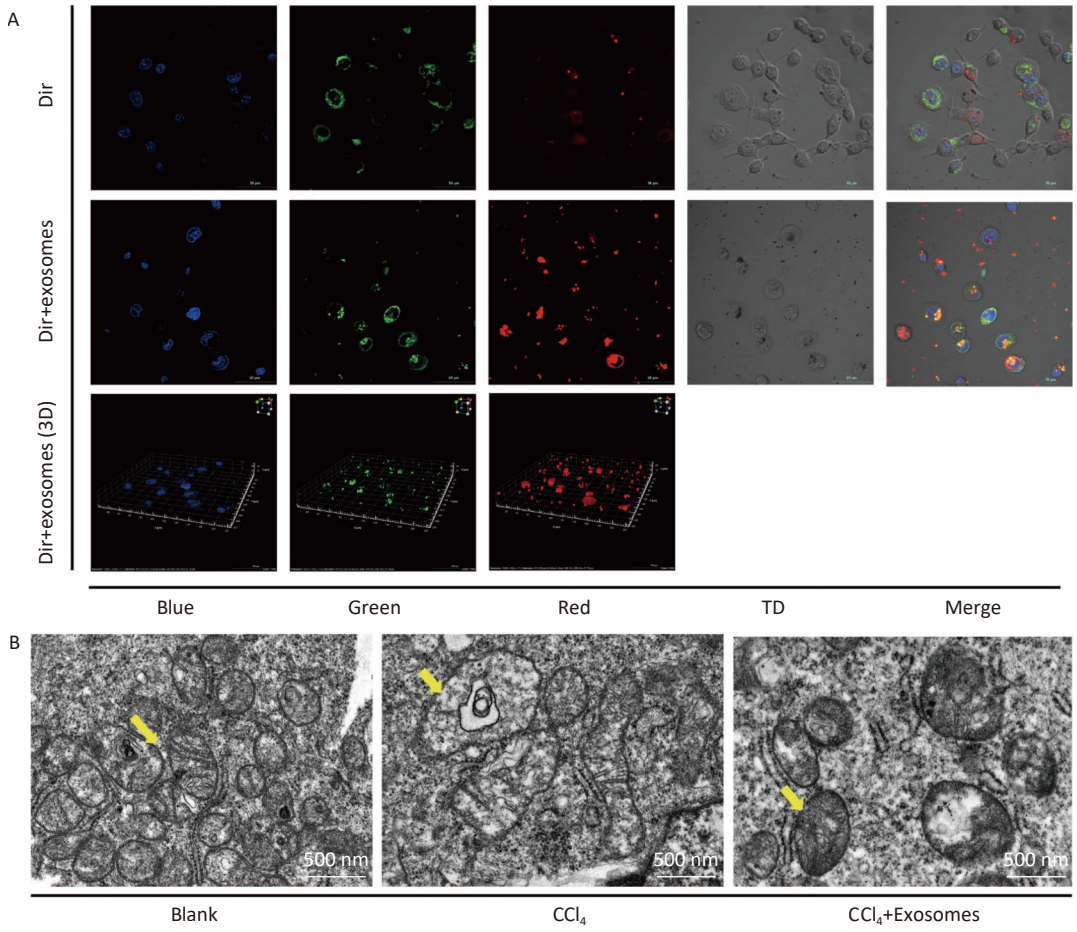


Fig.6 Cellular colocalization of exosomes with mitochondria and protective effects of exosomes on mitochondrial ultrastructure

A: three-color fluorescence colocalization analysis. Blue: cell nucleus (DAPI staining); green: mitochondria (MitoTracker labeling); red: DiR or DiR-labeled exosomes. TD: bright-field observation. In the DiR+ exosome group, the overlap of red and green signals produces an orange-yellow signal, and 3D fluorescence imaging confirms the spatial colocalization of the red signal (DiR+ exosomes) and the mitochondrial marker within the cell. B: transmission electron microscopy (TEM) observation of mitochondrial ultrastructure. The CCl_4 group shows disruption of the mitochondrial cristae structure, while partial structural restoration is observed in the CCl_4+ exosome group.

发挥着关键作用[11]。线粒体是新生脂肪合成(de novo lipogenesis)过程中的关键参与者[12]。脂肪分解中,脂质甘油三酯被水解成甘油和脂肪酸后,后者通过 β-氧化这一分解代谢过程进一步代谢,该过程发生在肝细胞线粒体中。此过程既可在脂解作用后直接发生,也可在脂肪酸进入线粒体前,先经过氧化物酶体 β-氧化缩短其极长链和多不饱和脂肪酸链[13]。

线粒体膜完整性对于维持正常的线粒体功能至关重要。线粒体通透性转换孔(mitochondrial permeability transition pore, MPTP)的开放会导致线粒体膜通透性发生改变,进而显著影响 ATP 合成、ATP 水平及细胞内钙离子浓度,进而引发细胞坏死[14];同时会导致线粒体肿胀及膜破裂,释放促凋亡因子并启动凋亡程序[15]。

通过代谢组数据分析挖掘,CCl_4+外泌体组与 CCl_4 组中的差异代谢物主要富集在初级胆汁酸生物合成通路,外泌体处理后可以降低脱氧胆酸(deoxycholic acid, DCA)和甘氨脱氧胆酸(glycodeoxycholic acid, GDCA)的丰度,而 DCA 能够插入线粒体内膜导致 MPTP 的开放,破坏线粒体膜电位,从而大量生成超氧阴离子($\cdot O_2^-$)等活性氧(reactive oxygen species, ROS)攻击细胞膜和细胞器膜上的不饱和脂肪酸,启动脂质过氧化[16]。GDCA 可作为急性肝衰竭患者的预后生物标志物之一[17],其通过脂质过氧化作用增加 MDA 水平,改

变肝细胞膜流动性，从而导致不同程度的肝细胞损伤[18]。提示外泌体可能通过下调 DCA 和 GDCA 重塑肝细胞的线粒体代谢和氧化还原能力，从而减轻 CCl_4 对肝细胞的损伤，相关潜在研究值得深入探讨。本研究荧光共定位分析中观察到外泌体与线粒体共定位，提示外泌体可能通过递送特定调控分子（如 miRNA 或蛋白）至线粒体，调节胆汁酸代谢相关酶（如 CYP27A1 等）或线粒体呼吸链复合物活性，从而改善线粒体功能，降低氧化应激，最终导致胆汁酸谱正常化。

同时，经外泌体干预后，对比 CCl_4 组，CCl_4+外泌体组恢复了维生素 B_3 在肝细胞中的水平，而维生素 B_3 是合成烟酰胺腺嘌呤二核苷酸（nicotinamide adenine dinucleotide, NAD^+）的前体。NAD^+作为底物直接参与氧化磷酸化（oxidative phosphorylation, OXPHOS）和电子传递链（electron transport chain, ETC）中，是维持线粒体稳态的关键辅助因子[19]。NAD^+还通过多种动态协调的稳态通路维持其他线粒体功能，包括调控 ROS 生成机制[20]、线粒体更新或线粒体自噬[21]，以及线粒体未折叠蛋白反应[22]。结合透射电镜结果，提示干细胞外泌体通过特征代谢物稳定线粒体结构与功能，从而维护肝细胞的正常状态。

HUMSCs 来源的外泌体显著纠正了 CCl_4 诱导的肝细胞 AST、ALT 和 MDA 水平异常及细胞活性下降。上述结果表明外泌体可能通过调节脂肪酸和线粒体代谢保护肝细胞的正常代谢与功能。

参考文献

[1] Jacques G, Sensébé Luc. Mesenchymal stromal cells: clinical challenges and therapeutic opportunities [J]. Cell Stem Cell, 2018, 22(6): 824-833.

[2] Liang X, Zhang Y, Ding Y, et al. Paracrine mechanisms of mesenchymal stem cell-based therapy: current status and perspectives [J]. Cell Transplantation, 2013, 23(9): 1045.

[3] Karantalis V, Hare JM. Use of mesenchymal stem cells for therapy of cardiac disease [J]. Circ Res, 2015, 116(8): 1413-1430.

[4] 李光宇, 周庆, 李宏达, 等. 间充质干细胞来源外泌体在肝纤维化中的治疗机制 [J]. 安徽医药, 2025, 29(4): 641-647.

[5] Kovach TK, Dighe AS, Lobo PI, et al. Interactions between MSCs and immune cells: implications for bone healing [J]. J Immunol Res, 2015, 2015: 1-17.

[6] Mortada I, Mortada R. Epigenetic changes in mesenchymal stem cells differentiation [J]. Euro J Med Gene, 2017: S1769721217304445.

[7] Zhao Z, Lin CY, Cheng K, et al. siRNA- and miRNA-based therapeutics for liver fibrosis [J]. Transl Res, 2019, 214: 17-29.

[8] Shao M, Xu Q, Wu Z, et al. Exosomes derived from human umbilical cord mesenchymal stem cells ameliorate IL-6-induced acute liver injury through miR-455-3p [J]. Stem Cell Res Thera, 2020, 11(1): 191.

[9] Br VK, Sarin SK. Acute-on-chronic liver failure: terminology, mechanisms and management [J]. Clin Mol Hepatol, 2023, 29(3): 670-689.

[10] Dai C, Xiao X, Li D, et al. Chloroquine ameliorates carbon tetrachloride-induced acute liver injury in mice via the concomitant inhibition of inflammation and induction of apoptosis [J]. Cell Death Dis, 2018, 9(12): 1136-1142.

[11] Mihajlovic M, Vinken M. Mitochondria as the target of hepatotoxicity and drug-induced liver injury: molecular mechanisms and detection methods [J/OL]. Int J Mol Sci, 2022, 23(6): 3315.

[12] Morio B, Panthu B, Bassot A, et al. Role of mitochondria in liver metabolic health and diseases [J]. Cell Calcium, 2020, 94: 102336.

[13] Poirier Y, ANtonenkov VD, Glumoff T, et al. Peroxisomal beta-oxidation-a metabolic pathway with multiple functions [J]. Biochim Et Biophys Acta Mol Cell Res, 2006, 1763(12): 1413-1426.

[14] Picard M, Taivassalo T, Ritchie D, et al. Mitochondrial structure and function are disrupted by standard isolation methods [J]. PLoS ONE, 2011, 6(3): e18317.

[15] Bernardi P, Gerle C, Halestrap AP, et al. Identity, structure, and function of the mitochondrial permeability transition pore: controversies, consensus, recent advances, and future directions [J]. Cell Death Diff, 30(8): 1869-1885.

[16] Palmeira CM, Rolo AP. Mitochondrially-mediated toxicity of bile acids [J]. Toxicology, 2004, 203(1-3): 1-15.

[17] Woolbright BL, McGill MR, Staggs VS, et al. Glycodeoxycholic acid levels as prognostic biomarker in acetaminophen-induced acute liver failure patients [J]. Toxicol Sci, 2014, 142(2): 436-444.

[18] Huang WF, Kang GF, Tu ZG. Glycodeoxycholic acid

changes the membrane fluidity and superoxides of lipids in hepatocytes [J]. Chin J Hepatol, 1999, 7(1): 46-47.

[19] Nolfi-Donegan B, Baseler WA, Bowman CE, et al. Mitochondrial electron transport chain: oxidative phosphorylation, oxidant production, and methods of measurement [J]. Redox Biol, 2020, 37: 101674.

[20] Juan CA, Pérez De La Lastra JM, Plou FJ, et al. The chemistry of reactive oxygen species (ROS) revisited: outlining their role in biological macromolecules (DNA, lipids and proteins) and induced pathologies [J]. Int J Mol Sci, 2021, 22(9): 4642.

[21] Ma K, Chen G, Li W, et al. Mitophagy, mitochondrial homeostasis, and cell fate [J]. Front Cell Devel Biol, 2020, 8: 467.

[22] Shpilka T, Haynes CM. The mitochondrial UPR: mechanisms, physiological functions and implications in ageing [J]. Nat Rev Mol Cell Biol, 2018, 19(2): 109.

Mechanism of stem cell exosome-mediated repair of hepatocyte injury via mitochondrial and fatty acid metabolism

YIN Xinxin[1], XIE Changpeng[1], LI Xuejing[1], ZHANG Liping[1], SU Zhanhai[1], WANG Haiyan[1], WU Qiong[1], PAN Yuanming[2], AN Juan[1]

[1] Department of Basic Medicine, School of Medicine, Qinghai University, Xining 810016, Qinghai, China; [2] Cancer Research Center, Beijing Chest Hospital Affiliated to Capital Medical University, Beijing 101149, China

ABSTRACT **AIM**: To investigate the metabolic mechanism by which umbilical cord mesenchymal stem cell exosomes repair CCl_4-induced acute liver injury and to analyze the role of key metabolites in regulating the repair process. **METHODS**: The experiment was divided into three groups: the CCl_4 group, the CCl_4+low-dose exosome group, and the CCl_4+high-dose exosome group. Cell viability of HL-7702 cells, as well as levels of AST, ALT, and MDA, were measured. Targeted metabolomics analysis was performed to identify differential metabolites between the CCl_4 group and the CCl_4+exosome group. The co-localization relationship between exosomes and the nucleus or mitochondria in HL-7702 cells was observed using confocal laser scanning microscopy. Mitochondrial structural changes in each group were examined by transmission electron microscopy. **RESULTS**: Exosomes significantly reversed the decline in cell viability induced by 25 mmol/L CCl_4. Additionally, exosomes markedly reduced AST, ALT, and MDA levels. A total of 73 significantly differential metabolites were identified between the CCl_4 group and the CCl_4+exosome group, including glycodeoxycholic acid and tetradecanedioic acid. Fluorescence staining revealed co-localization of exosomes with both the nucleus and mitochondria. **CONCLUSION**: Exosomes significantly reversed the abnormal levels of AST, ALT, and MDA induced by CCl_4 in HL-7702 cells and protected mitochondrial structure against oxidative stress damage. Metabolomic findings suggest that exosomes may repair hepatocyte injury by mediating mitochondrial function and fatty acid metabolism.

KEYWORDS liver injury; exosomes; mitochondria; fatty acid metabolism; metabonomics